Materials Advances

ROYAL SOCIETY OF CHEMISTRY

PAPER

View Article Online
View Journal | View Issue

Cite this: *Mater. Adv.*, 2023, 4, 6645

Computational study of the physical characteristics of Si-based oxide perovskites for energy generation using DFT

Amjad Ali Pasha,[a] Hukam Khan,[b] Mohammad Sohail,*[a] Nasir Rahman,[b] Rajwali Khan,[b] Omar H. Alsalmi,[c] Dilsora Abduvalieva,[d] Khamael M. Abualnaja,[e] Atef El Jery[f] and Mouataz Adrdery[f]

$SiMO_3$ (M = Sn, Ge) silicon-based oxide perovskite compounds are studied using density functional theory (DFT) and Wien2k software to examine their structural, elastic, optical, and electronic properties. The Birch–Murnaghan equation is used to optimize $SiSnO_3$ and $SiGeO_3$ compounds and deliver structural stability, whereas the IRelast program is used to find elastic constants to confirm the flexible stability as well as the elastic behavior of the presented compounds. These compounds resist plastic strain and are ductile, scratch resistant, anisotropic, and mechanically stable. The Trans-Blaha modified Becke–Johnson potential approximation calculations demonstrate that the band structure of $SiSnO_3$ is intermetallic, whereas the second compound, $SiGeO_3$, is a semiconductor. The evidence obtained from the band structure and density of states of the these compounds demonstrates that $SiSnO_3$ has an indirect band gap, and the minima of the conduction band are at evenness point *X*, whereas the maxima of the valence band are at symmetry points *M*, resulting in an indirect band gap (*X*–*M*). Meanwhile, $SiGeO_3$ has a direct band gap, and the minima of the valence band and maxima of the conduction band occur at symmetry points *X*. These crystals have low-energy absorption. If we examine the reflectance of ternary molecules $SiGeO_3$ has a low absorption of up to 2 eV with fluctuations and the absorption increases to a maximum value of 40.0 at 6.50 eV. In contrast, $SiSnO_3$ exhibits a different increase, and the absorption coefficient decreases to the lowest value of 12.4 eV. Our optical property analysis showed that $SiSnO_3$ and $SiGeO_3$ can be used in high-frequency ultraviolet devices. To the best of our knowledge, this is the first DFT-based examination of the characteristics of these crystals.

Received 11th August 2023,
Accepted 5th November 2023

DOI: 10.1039/d3ma00537b

rsc.li/materials-advances

1. Introduction

Energy a basic need of every human being, is available to everyone, on average, in decreasing amounts over time. Perovskites are crystals used in generating and storing energy, and therefore, they remain popular among researchers. To produce perovskites with better properties, researchers are trying to make new perovskites. The typical chemical formula for perovskites is ABX_3, where X may be oxygen, fluorine, chlorine, bromine, or iodine. Components A and B are cations, and X is an anion. $CaTiO_3$ was the first material found, which obeyed this formula. Each perovskite structure is arranged in a way that twelve atoms of cation A and six atoms of cation B are bound to the anion. Oxide perovskites are found in the form of insulators, conductors, and semiconductors. These compounds can have stable crystalline structures with excellent electronic properties. These materials have applications in the lens industry, lithography, photoelectric materials, and energy storage devices.[1–3] Several studies have been conducted revealing the various characteristics of perovskite crystals, especially oxide perovskites, which remain of great interest. Majority of researchers have concluded that they are mechanically and elastically stable.[4–6] These crystals are promising for highly effective photovoltaic components and superior energy storage applications in automobiles, electronics, and optics.[7–9] Oxygen is combined with inorganic species, organic species, or metals

[a] *Faculty of Engineering, Aerospace Engineering Department, King Abdulaziz University, P.O. Box 80204, Jeddah-21589, Saudi Arabia. E-mail: msohail@ulm.edu.pk*
[b] *Department of Physics, University of Lakki Marwat, Lakki Marwat 28420, Khyber Pakhtunkhwa, Pakistan*
[c] *Physics Department, Faculty of Applied Science, Umm AL-Qura University, Makkah 24382, Saudi Arabia*
[d] *Doctor of Philosophy in Pedagogical Sciences, Tashkent State Pedagogical University, Bunyodkor avenue, 27, Tashkent, 100070, Uzbekistan*
[e] *Department of Chemistry, College of Science, Taif University, Taif 21944, Saudi Arabia*
[f] *Department of Chemical Engineering, College of Engineering, King Khalid University, Abha 61411, Saudi Arabia*

from the transition metal group to produce stable oxide perovskites. Wide band gap oxide perovskites are most viable. Such molecules can be employed to generate glass that operates in the vacuum ultraviolet and UV spectra due to their large energy band gap and high potential.[10,11] Some new investigations on oxide perovskites have been conducted.[12–14] Harmel *et al.*[15] used density functional theory (DFT) to examine the characteristics of $BaCsO_3$ oxide perovskites based on barium. They concluded that $BaCsO_3$ will be suitable for electrooptic instruments because of its widespread direct band gap and bands of the imaginary constituent of the nonconducting features in the UV range. Daniel *et al.*[16] demonstrated that the characteristics of LiBaO3 are effective for energy storage. Compounds with band gaps of >3.10 eV will be effective in the UV spectrum. $SiSnO_3$ with intermetallic character and $SiGeO_3$ with semiconductor properties are excellent candidates for electronic applications. Herein, with the help of DFT and the full-potential linear augmented plane wave (FP-LAPW) method, we discuss some fundamental characteristics of $SiMO_3$ (M = Sn, Ge) oxide perovskites, providing insights for further research. These properties include structural, elastic, electronic, and optical properties.

2. Computational methodology

To calculate the above-mentioned characteristics, the FP-LAPW approach was used with the help of Wien2k software, and the results were discussed.[17–22] We used the Trans-Blaha modified Becke–Johnson (TB-mBJ) technique, because it is useful in calculating the density of states (DOS) and optical and electronic properties.[23] For the calculation of structural and elastic properties, generalized gradient approximation (GGA) and the exchange–correlation potential were applied as they are useful tools for such calculations.[24] This study includes the investigation of some FP-LAPW base functions for which the value of muffin-tin radius (RMT) spheres was chosen to be 8. In our model, K_{max} in the plane wave expansion is the magnitude of the supreme K points to attain a high degree of convergence. The RMT values for M and O are 2.38, 1.73, and 1.67 atomic units (a.u.), respectively. Within the muffin-tin spheres, the spherical harmonics were increased to $l_{max} = 11$, whereas the Fourier expanded charge density was decreased to $G_{max} = 12$ (a.u.). The self-consistent field computations were considered to have converged, as the total energy dropped within the energy range of 0.0001 Ry. By equating the energy against volume curve, the equation of state by Birch–Murnaghan was used.[25,26] To calculate the elastic constant used in analyzing the structural properties, we used the IRelast software.[26] Additionally, we used the dielectric function $\varepsilon(\omega)$ to investigate the optical behavior of our selected crystals.[27,28]

3. Results and discussion

This section of the article provides a thorough scientific analysis of the results generated by our TB-mBJ potential approach. We will discuss structural and optical characteristics using this approach.

3.1 Structural properties

$SiMO_3$ are the chosen crystals for investigation. The space group of our selected crystals is $Pm\bar{3}m$ number 221. It has a cubic unit cell structure comprising a single molecule and obeys the ABO_3 formula, which means the crystals are oxide perovskites. The arrangement of atoms in the unit cell is such that Si atoms occupy (0, 0, 0) positions, M atoms at $(1/2, \frac{1}{2}, \frac{1}{2})$, and oxygen atoms at (0, 1/2, 1/2), (1/2, 0, 1/2), and (1/2, 1/2, 0), as shown in Fig. 1. We will compute the total energy around V_o in terms of the unit cell volume (the volume of the cell at the equilibrium point). For computing the volume optimization, to possibly predict the structural behavior of our selected crystals, we will utilize the Birch–Murnaghan's equation of state.[25] To get the lowest stable unit cell, we will reduce the overall energy of the unit cell. The data derived from Birch–Murnaghan's equation of state are analytically estimated to predict the ground state characteristics of the unit cell. These include the equilibrium lattice constant a_o, the bulk modulus B, and its pressure derivative B'.

The minimum energy E_o, for which the volume gets its lowest value V_o, gives the actual minimum ground state of that particular compound. Those crystals that have more negative energy have more stable structures. The optimized structural parameters such as a_o, E_o, V_o, B_o, and B' are tabulated in Table 1. These results are reliable with the general trend indicating that as the bulk modulus drops, the lattice constant increases, which shows that the computed results are precise and accurate. The optimization graphs demonstrate that $SiSnO_3$ has more negative energy, indicating more structurally stability than $SiGeO_3$, as shown in Fig. 2 and Table 1.

3.2 Electronic properties

Herein, we determine the real maps of the band structures, DOS, and arrangement of charge to analyze the electronic state of $SiMO_3$ molecules. Local density approximation and GGA calculations significantly underestimate the essential band gaps of semiconductors and dielectrics.[29,30] This is because the exchange–correlation energy and the charge derivative

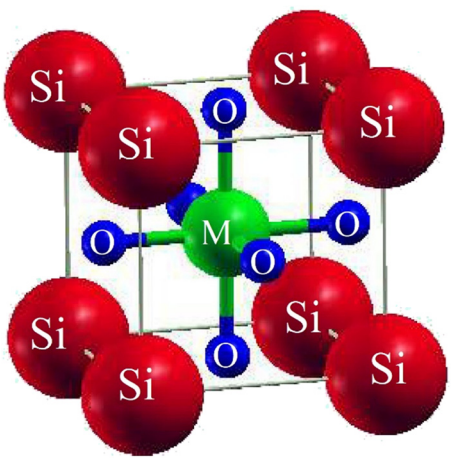

Fig. 1 Conventional cubic crystal structure of $SiMO_3$ ternary molecules.

Table 1 Optimized crystal unit cell computed data of $SiMO_3$ molecules

Compound	a_o (Å)	B (GPa)	B'	V_0 (a.u.^{3})	E_0 (Ry)
$SiSnO_3$	3.72	202.32	4.59	346.37	−13390.08
$SiGeO_3$	3.61	221.05	4.47	318.70	−5229.98

cannot be consistently reconstructed by the basic structure. TB-mBJ is effectively applied in various research reports[14,31,32] and is selected to solve the underestimation of the band gaps. In the higher symmetry direction of the Brillouin zone, the energy-band structures obtained for the symmetric geometry of $SiMO_3$ are shown in Fig. 3. The valence band and conduction band are separated by a horizontal line, which represents the Fermi energy level, E_F. Above the Fermi level, there is the conduction band, and the valence band is shown below the Fermi level. According to Fig. 3a, $SiSnO_3$ and $SiGeO_3$ are semiconductors, because their energy band gaps lie between 0 and 3.1 eV. $SiSnO_3$ has an indirect (M–X) energy state gap of 2.4 eV, and $SiGeO_3$ has a direct (X–X) energy gap of 3.1 eV. We usually calculate the spin orbit coupling (SOC) for an element used in a compound having an atomic number of >50. We calculated the band structure using SOC calculation with TB-mBJ and found no change in the energy band gap in the band structures of both these compounds as shown in Fig. 3b.

To gain a greater understanding of the electronic states of $SiMO_3$ crystals, the total density and partial density of states (TDOS and PDOS, respectively) are calculated as depicted in Fig. 4a. Each band consists of a vertical line representing a zero level, called the Fermi level. The left side of each band represents the valence band, whereas the right side is devoted to the conduction band. The roles of different electronic states in the valence and conduction bands are represented by their respective lines labeled in each graph of Fig. 4a. The energy range for the DOS of $SiGeO_3$ is −12.5 to 7 eV, whereas for $SiSnO_3$ is −9 to 7 eV. Some of the major influences of different states in the valence and conduction bands are explained as follows: First, we present the details of $SiSnO_3$. The major contribution in the valence band is from O-tot, which is −4.4 to 0 eV, with the highest peak of 2.8 corresponding to −1 eV. Other peaks observed for the same states are 1.8, 2, and 2.6 at −1.5, −1.2, and −0.6 eV, respectively. The second highest contribution in the same band is from the Si-s state, with a value of 2 at −5.8 eV. The contributions from all other states are minor, such as the Sn-d state, whose value is approximately 0.2 in the energy range of −3.1 to 0.3 eV. For the same compound in the conduction band, the Si-p state has a maximum contribution from 3.2 to 5 eV with the highest peak of 3.3 at 4.5 eV. The contribution of O-tot is from 3.6 to 4.6 eV, having a peak of 0.4 at 4.5 eV. Secondly, an explanation of the DOS of $SiGeO_3$ is as follows: The O-s state has a major contribution in the valence band with an energy range of −6 to 0 eV. It has different peaks at different energy levels, such as 0.5, 0.6, and 1.5 at −7.5, −6, and −2.5 eV, respectively. The Ge-s state in the same band has peaks of 0.7 and 0.8 at −7.5 and −1 eV, respectively. O-tot and Si-tot have some contribution, but it is minimal. Similarly, in the conduction band of $SiGeO_3$, Ge-p has the highest contribution, with peaks 0.6 and 1.7 at 4.9 and 6 eV, respectively. Other contributions are from Ge-tot and O-s states, which have very small values.

3.3 Elastic properties

The reactions to exterior forces by a particular compound are used to compute the flexible properties of that compound. The obtained data from such calculations give evidence regarding the stability and toughness of the crystal. By finding the components of stress tensor for tiny deformations and determining the energy in accordance with the lattice distortion that preserves the volume, the elastic factors of the compounds were determined with no pressure.[33] For finding the elastic constants, the IRelast program was used with the help of the Wien2k software, thereby using all the particulars of the cubic system. The important elastic constants from which we can get detailed information of any cubic crystal system are C_{11}, C_{12}, and C_{44}. These elastic constants

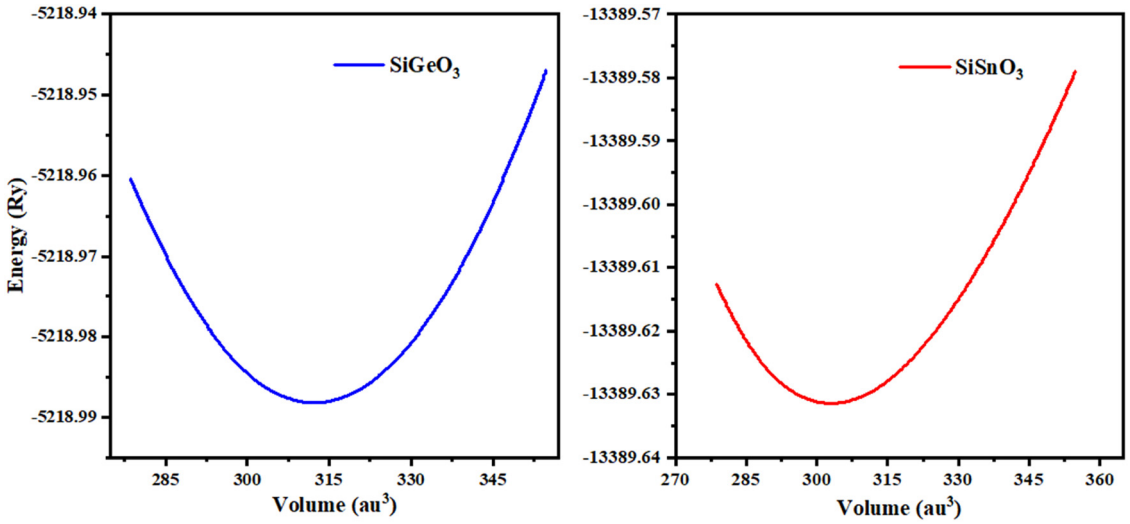

Fig. 2 Optimization curves of $SiMO_3$ crystals fitted by Birch–Murnaghan's equation of state.

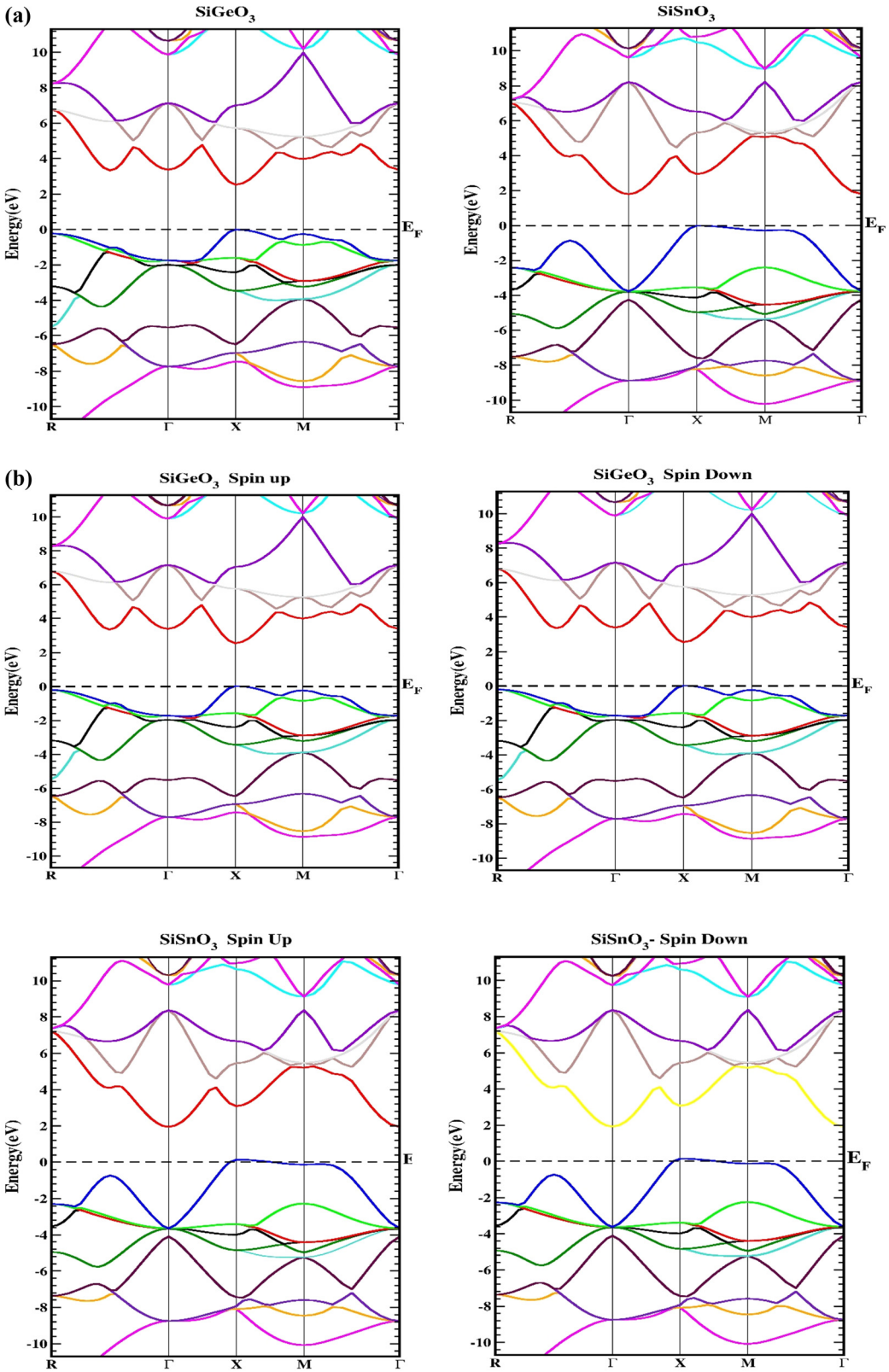

Fig. 3 (a) Representation of the band structures of $SiMO_3$ using TB-mBJ approximation. (b) Representation of the band structures of $SiMO_3$ using TB-mBJ with SOC.

are independent of each other and are presented in Table 2. To have a mechanically stable cubic crystal, the elastic constants should satisfy the following conditions: $C_{11} > C_{12}$, $C_{11} > 0$, $C_{44} > 0$, $C_{11} + 2C_{12} > 0$, and $B >$ zero.[34] The phonon calculation, as

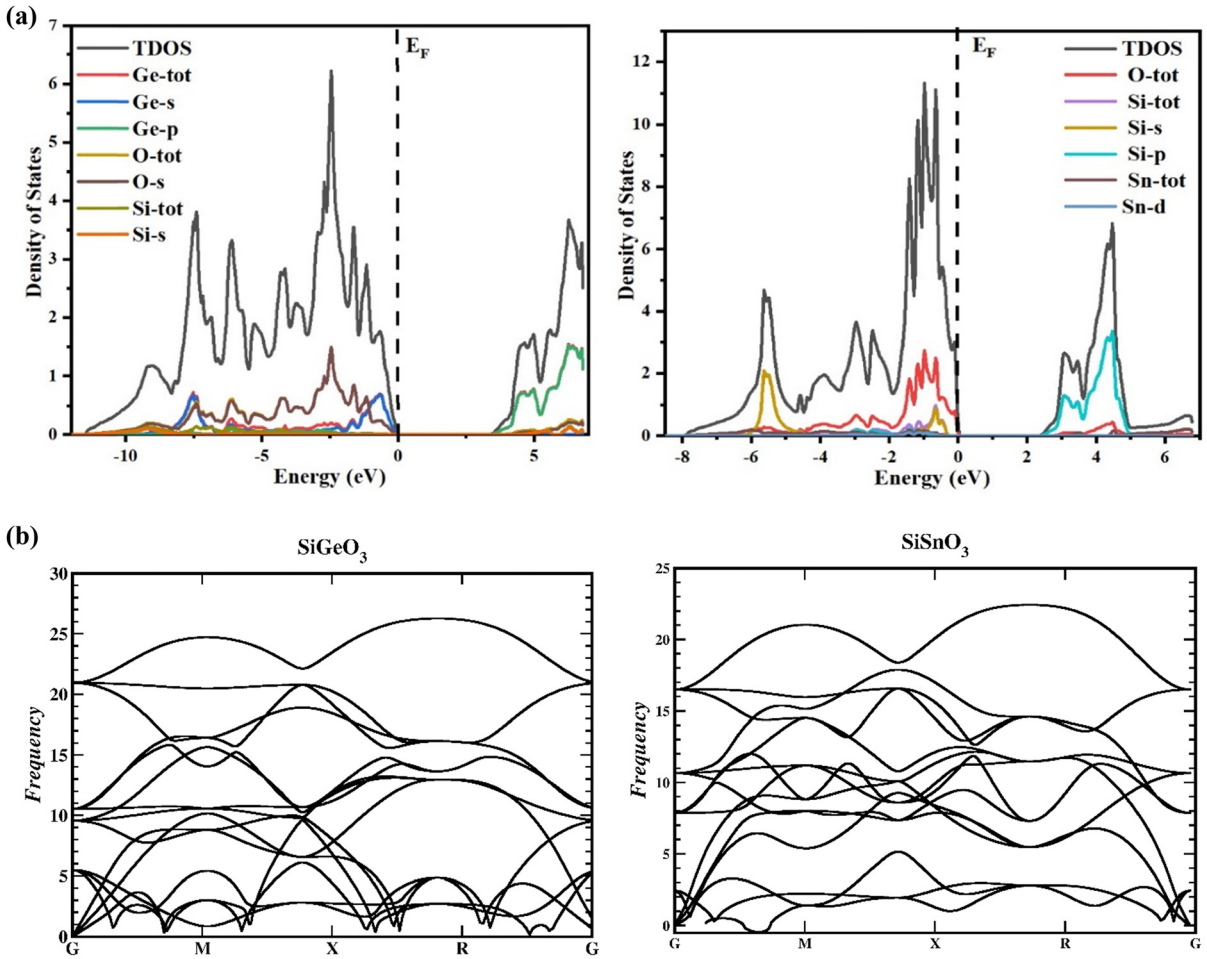

Fig. 4 (a) TDOS and PDOS of $SiMO_3$ crystals using TB-mBJ approach. (b) Representation of the phonon band structures of $SiMO_3$.

depicted in Fig. 4b, demonstrate that there is no imaginary frequency and all the observed frequencies are real for $SiSnO_3$ and $SiGeO_3$, verifying that these compounds exhibit thermodynamic stability.[35,36]

The above-mentioned conditions are satisfied for our calculated elastic constants, indicating that these compounds are mechanically stable. According to our calculated data, the C_{11} value of $SiSnO_3$ is 202.3236 GPa and that of $SiGeO_3$ is 221.0451 GPa, which proves that $SiGeO_3$ is to some extent stiffer than $SiSnO_3$. Another parameter, known as the anisotropic constant, represented by A, gives information regarding the capacity of a crystal to produce small fractures. Engineers normally use this information to study the microscopic behavior of a crystal in response to external stress. The values of A for our selected compounds are calculated from the above-mentioned elastic constants with the help of the formula mentioned below.

$$A = 2 \times C_{44}/C_{11} - C_{12} \quad (1)$$

The material will be isotropic if the value of $A = 1$, otherwise it will be anisotropic. The calculated values of A for both of our compounds are depicted in Table 2.

Both the compounds are anisotropic, since the value of A deviates from 1 and the degree of variance reveals the degree of anisotropy. As it is clear from Table 2, the calculated value of A for $SiSnO_3$ is 0.515 and that of $SiGeO_3$ is 2.305, which shows that $SiSnO_3$ is less anisotropic than $SiGeO_3$. Other important parameters such as the Young's modulus represented by E, the shear modulus represented by G, and Poisson's ratio represented by ν are calculated with the help of the elastic constants, tabulated in Table 2. Below are the formulae used to obtain these parameters.[37–39]

$$E = \frac{9 \times B \times G}{G + 3 \times B} \quad (2)$$

Table 2 Few important constants of $SiMO_3$ molecules

Compound	$SiSnO_3$	$SiGeO_3$
C_{11}	247.05	327.52
C_{12}	76.59	175.45
C_{44}	43.89	175.28
G	57.44	125.37
A	0.56	2.31
V	0.34	0.19
B/G	2.99	1.37

$$v = \frac{3 \times B - 2 \times G}{2(G + 2 \times B)} \quad (3)$$

$$G_v = \frac{C_{11} - C_{12} + 3 \times C_{44}}{5} \quad (4)$$

$$G_R = \frac{5 \times C_{44}(C_{11} - C_{12})}{4 \times C_{44} + 3C_{11} - C_{12}} \quad (5)$$

Ductility and brittleness are important characteristics in the study of the structure of any particular crystal. The Cauchy pressure, C_{11}–C_{44}, can indicate the ductility of a crystal.[40] If the difference between these constants is positive, the material will be ductile, otherwise brittle. Both of our crystals have positive Cauchy pressures, 8.63382 GPa for $SiSnO_3$ and 8.7825 GPa for $SiGeO_3$, showing that they both exhibit ductility. Therefore, our selected $SiMO_3$ crystals are mechanically ductile, anisotropic, tough, and fracture resistant. Materials with such characteristics have vast applications in the field of modern technology.

3.4 Optical properties

To calculate the optical properties of our selected crystals, we used incident photons with energy ranges from zero to 14 eV, using the estimated equilibrium lattice constant and the dielectric function $\varepsilon(\omega)$ to obtain all the optical characteristics of both crystals.

3.4.1 Dielectric function. The dielectric function is represented by $\varepsilon(\omega)$ and given by the equation $\varepsilon(\omega) = \varepsilon_1(\omega) + i\varepsilon_2(\omega)$. It consists of two parts. The first part represents the real part, and the second part represents the imaginary part. Fig. 5 demonstrates the distribution of incoming photons for the crystals and electronic polarizability. The real part of $SiGeO_3$ starts from 4.3 at 0 eV and increases to 9.5 at 5.2 eV; it then decreases to 3.6 at 5.5 eV. At 6 eV, its value gets little greater and reaches 4, after which it decreases with fluctuating values and shows the lowest value of −1.9 at 9 eV, and its value reaches zero (approximately) at 12.5 eV. The imaginary part of the same crystal starts from zero at 0 eV and remains at zero until it reaches an energy value of 3.5 eV. It then increases to the highest value of 8 at 5.5 eV. Other peaks observed for the same part of the same compound are 7.5, 4, and 1.7 at 6, 9, and 13.5 eV, respectively. It is also clear from the same graph that the real part of $SiSnO_3$ shows a value of 4.4 at 0 eV, and upon increasing the energy, its value increases to a maximum value of 7.6 at 4.5 eV. The graph summarizes that the value remains fluctuating until 14 eV with the following peaks: 5.5, 1.7, 0.1, and −2.5 at 5.3, 7.5, 9.5, and 13.5 eV, respectively. The imaginary part of the same compound is depicted in the same graph, starting from 0 at 0 eV, and has the same value up to the energy value of 3 eV. Further, its value increases to 7.8 at 5 eV and decreases to 4 at 4.5 eV, then increases again to 7.9 at 6.3 eV; we observe peaks at 5.8, 3.2, 3.5, 2.4, and 1.8 at 7.5, 9.5, 10, 11.6, and 13.5 eV, respectively. According to the Penn model, those crystals with a greater energy band gap result in smaller values of the static dielectric function.[41–45] Fig. 5 demonstrates that the behavior of the real parts of both crystals shows similar behavior at low, intermediate, and higher energies, and the same behavior is shown by their respective imaginary parts of the dielectric function $\varepsilon(\omega)$.

3.4.2 Refractive indices. From the calculated values of $\varepsilon_1(\omega)$ and $\varepsilon_2(\omega)$, we can derive values of different parameters for the calculation of different optical properties of any crystal, such as the refractive index represented by $\eta(\omega)$, conductivity represented by $\sigma(\omega)$, absorption coefficient represented by $I(\omega)$, and reflectivity represented by $R(\omega)$. Fig. 6 represents the computationally calculated values of the refractive indices of $SiMO_3$ crystals. The refractive index at 0.0 eV, $\eta(0)$, for $SiGeO_3$ is 2.1 and that of $SiSnO_3$ is 0.4. There is a large gap between the refractive indices $\eta(\omega)$ of both the compounds at all energies. Some prominent peaks of the refractive index of $SiSnO_3$ are 3.2, 1.5, and 0.7 at 5, 8.7, and 13.5 eV, respectively. The refractive index peaks of $SiGeO_3$ are 0.5, 0.4, and 0.5 at 5.5, 12, and 13.5 eV, respectively. The computed data analysis demonstrates that the refractive index of $SiSnO_3$ is >1, with a photon energy of ≤ 9.5 eV; compounds that possess large number of electrons are normally more refractive. Thus, any process which increases the electron density increases the refractive index.

3.4.3 Absorption coefficient. The absorption coefficient, $I(\omega)$, was calculated from the dielectric function, $\varepsilon(\omega)$, as shown in Fig. 7. It is evident that at 0 eV, both compounds have zero

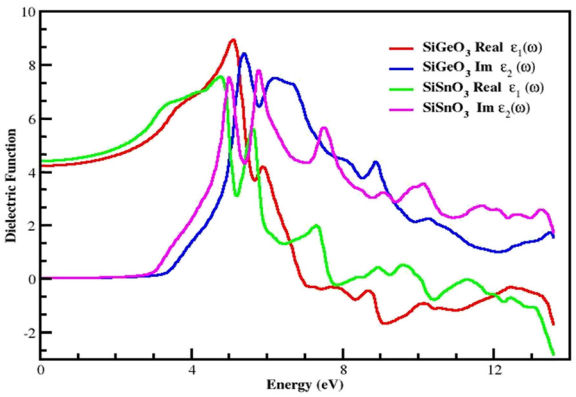

Fig. 5 Dielectric function $\varepsilon(\omega)$ of $SiMO_3$ molecules.

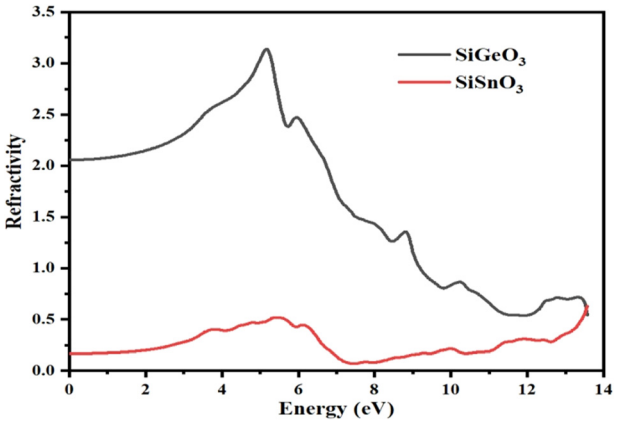

Fig. 6 Calculated refractive indices of compounds $SiMO_3$.

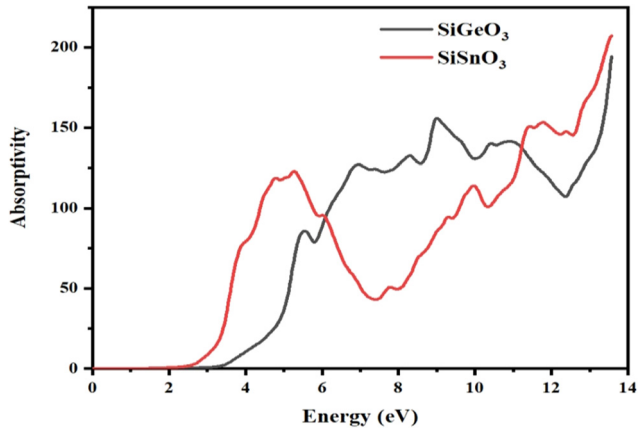

Fig. 7 Calculated absorption coefficient of crystals $SiMO_3$.

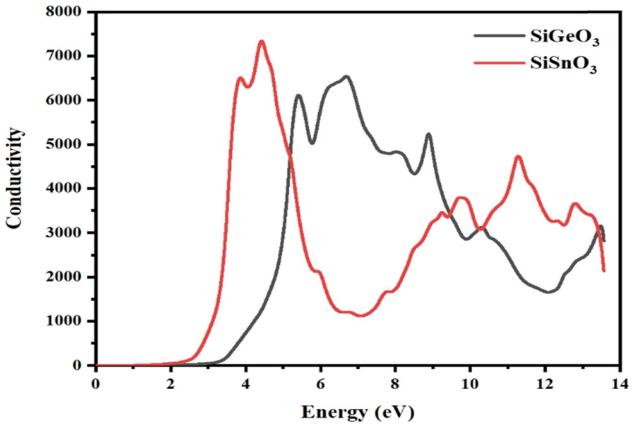

Fig. 9 The optical conductivity $\sigma(\omega)$ through $SiMO_3$ (M = Sn and Ge) compounds.

absorption coefficients, and they are zero until 2.7 eV for $SiSnO_3$ and 3.4 eV for $SiGeO_3$. This means that the threshold energy for $SiSnO_3$ is 2.7 eV and that for $SiGeO_3$ is 3.4 eV. Further, the absorptivity of both the compounds is nonzero and remains >45 for until 14 eV. The fluctuating values of $I(\omega)$ for $SiSnO_3$ are 140, 45, 100, 150, and 220 at 4.9, 7.3, 9.9, 11.3, and 13.5 eV, respectively. For $SiGeO_3$, the peaks are 70, 130, 150, and 195 at 5.5, 6.8, 9, and 13.5 eV, respectively. Therefore, from 2 to 6 eV, $SiSnO_3$ has good absorptivity; from 6 to 11.5 eV, $SiGeO_3$ has better absorptivity; and after that $SiSnO_3$ again has better absorptivity.

3.4.4 Reflectivity. The reflectivity of the crystals, $R(\omega)$, is derived from the dielectric function. The threshold values of both the compounds are nonzero and are 0.15 and 0.18 for $SiGeO_3$ and $SiSnO_3$, respectively. Some observed peaks for $SiSnO_3$ are 0.4, 0.51, and 0.66 at 3.6, 5.4, and 13.5 eV, respectively. For $SiGeO_3$, prominent peaks are 0.32, 0.35, 0.41, 0.42, and 0.55 at 5.3, 7, 9.1, 11.5, and 13.5 eV, respectively. The reflectances at zero-frequency $R(0)$ for $SiSnO_3$ and $SiGeO_3$ are 0.54 and 0.72, respectively. The greater the reflectivity of the crystal, the lesser the transparency. Upon comparing the reflectivity of both these compounds, $SiGeO_3$ is more transparent before 6.5 eV, after which $SiSnO_3$ is more transparent until 12 eV, and from 12 to 14 eV, $SiGeO_3$ is more transparent again as is depicted in Fig. 8. Those materials which have good transparency are recommended in making efficient lens materials.

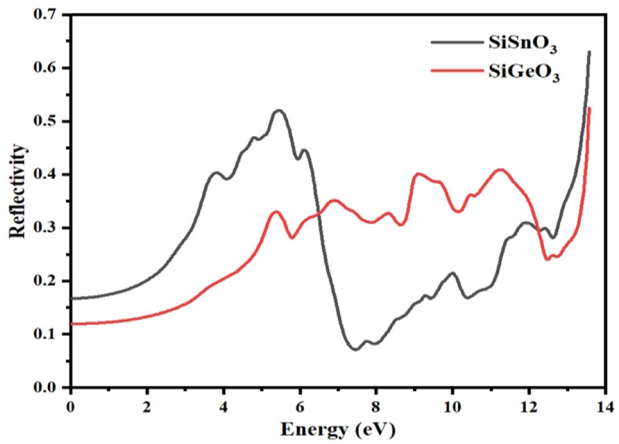

Fig. 8 Reflectivity $R(\omega)$ of incident light from the $SiMO_3$ crystals.

3.4.5 Optical conductivity. The optical conductivity $\sigma(\omega)$ is defined as the relationship between the induced current density and the absolute value of the induced electric field in the substance, at any particular frequency for any specific material. This property is used to represent the photon conduction inside a material. With the help of the dielectric function, as depicted in Fig. 9, for both of our selected crystals, the photon conductivity is zero at 0 eV and remains zero up to 2.4 eV, then the value for $SiSnO_3$ increases to 6700 at 3.4 eV and to the highest value of 7600 at 4.4 eV. Meanwhile, for $SiGeO_3$, the value remains zero until 3.1 eV; the value of the conductivity reaches 6400, 5000, 6600, 5400, 3100, and 3200 at 5.3, 5.9, 6.9, 8.8, 10.5, and 13.4 eV, respectively. Similarly, the value of the photon conductivity for $SiSnO_3$ decreases to 1000 from 7600 at 7 eV and increases to 4200 at 10 eV. After that, it decreases slightly at 10.3 eV, then another peak of 5000 at 12.5 eV. Therefore, in the energy range of 2.2 to 5 eV, $SiGeO_3$ is more conductive, whereas in the energy range of 5 to 9.5 eV, $SiSnO_3$ is more conductive, after which the situation reverses until 13.5 eV.

3.4.6 Energy loss function (ELF). The ELF demonstrates the energy lost by an electron when it moves through a particular compound. The same function may be used to define intraband, interband, and plasmon interdependence. Herein, the calculated energy loss by an electron as shown in Fig. 10 indicates that the ELF values for both of our selected compounds are zero from 0 to $\sim$2.9 eV. For $SiGeO_3$, the value remains zero until 3.5 eV. For $SiSnO_3$, after 2.9 eV, the value increases and reaches the highest value of 0.88 at 7 eV and decreases to 0.35 at 8.3 eV; other peaks are 0.44, 0.36, and 0.45 at 10.3, 11.2, and 12.5 eV, respectively. For $SiGeO_3$, the value of the ELF increases continuously from 3.5 to 12.2 eV at a varying rate with the following peaks: 0.12, 0.26, 0.39, and 0.9 at 5.8, 8.5, 10.1, and 12.2 eV, respectively. Thus, at low energy, both compounds do not absorb any electron energy; at the intermediate level, *i.e.*, from 6 to 8.2 eV, $SiSnO_3$ is an excellent

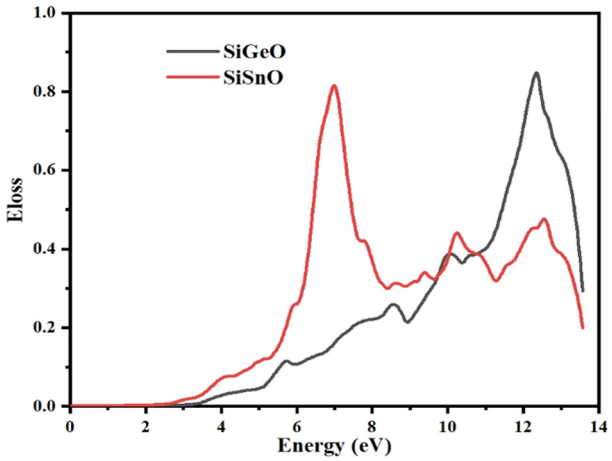

Fig. 10 Representation of the function for the loss of optical energy $L(\omega)$ of $SiMO_3$.

absorber of electron energy; whereas at higher energies, *i.e.*, from 10 to 12.2 eV, $SiGeO_3$ is a good absorber.

4. Conclusion

We computed the elastic, structural, optical, and electrical properties of $SiMO_3$ crystals. Harmony and coherence make our results more precise. Structural characteristics show that $SiMO_3$ crystals are cubic and stable. The basic elastic constant, anisotropy factor, Poison ratio, ductility, Cauchy pressure, shear modulus, Pugh ratio, and Young modulus are predicted by IRelast. Based on these fundamental elastic properties, both materials are ductile, anisotropic, elastically stable, and scratch resistant. These studies proved that these crystals can be employed in several electronics applications. The calculation of SOC with TB-mBJ demonstrated that $SiGeO_3$ is a semiconductor, and $SiSnO_3$ exhibits intermetallic properties. The TDOS and PDOS results are as follows: O-tot, with a peak of 2.8 at −1 eV, dominates $SiSnO_3$'s valence band. The same states have maxima at 1.8, 2, and 2.6 at −1.5, −1.2, and −0.6 eV, respectively. The Si-s state contributes 2 at −5.8 eV. The Si-p state contributes most to the conduction band of the same crystal, with a peak of 3.3 at 4.5 eV. The contribution of O-tot is from 3.6 to 4.6 eV, with a peak of 0.4 at 4.5 eV. For $SiGeO_3$, in the valence band, the O-s state has the major contribution in the energy range from −6 to 0 eV. It has different peaks at different energy levels, such as 0.5, 0.6, and 1.5 at −7.5, −6, and −2.5 eV, respectively. The Ge-s state in the same band has peaks of 0.7 and 0.8 at −7.5 and −1 eV, respectively. In the conduction band, Ge-p has the largest contribution with peaks of 0.6 and 1.7 at 4.9 and 6 eV, respectively. Further, due to a low absorption coefficient, optical property analysis demonstrated that $SiSnO_3$ and $SiGeO_3$ can be used in high-frequency UV devices. To the best of our knowledge, this is the first DFT-based examination of the characteristics of these crystals.

Data availability

This manuscript has no associated data.

Conflicts of interest

The authors have no conflict of interest.

Acknowledgements

This work was supported by the King Khalid University, Abha, Saudi Arabia. The authors extend their appreciation to the Deanship of Scientific Research at King Khalid University for funding this work through Large Groups Project under grant number (R.G.P. 2/43/44).

References

1 T. Nishimatsu, N. Terakubo, H. Mizuseki, Y. Kawazoe, D. A. Pawlak, K. Shimamura and T. Fukuda, Band structures of perovskite-like fluorides for vacuum-ultraviolet-transparent lens materials, *Jpn. J. Appl. Phys.*, 2002, **41**, L365.
2 C. Dotzler, G. Williams and A. Edgar, $RbCdF_3:Mn^{2+}$: a potential ultraviolet dosimeter material, *Appl. Phys. Lett.*, 2007, **91**, 181909.
3 G. Vaitheeswaran, V. Kanchana, R. S. Kumar, A. L. Cornelius, M. F. Nicol, A. Svane, A. Delin and B. Johansson, High-pressure structural, elastic, and electronic properties of the scintillator host material $KMgF_3$, *Phys. Rev. B: Condens. Matter Mater. Phys.*, 2007, **76**, 14107.
4 S. Naeem, G. Murtaza, R. Khenata and M. Khalid, First principle study of $CsSrM_3$ (M = F, Cl), *Phys. B*, 2013, **414**, 91–96.
5 A. Mubarak, *Ab initio* study of the structural, electronic and optical properties of the fluoropervskite $SrXF_3$ (X = Li, Na, K and Rb) compounds, *Comput. Mater. Sci.*, 2014, **81**, 478–482.
6 A. Mubarak and S. Al-Omari, First-principles calculations of two cubic fluoropervskite compounds: $RbFeF_3$ and $RbNiF_3$, *J. Magn. Magn. Mater.*, 2015, **382**, 211–218.
7 R. Khan, K. Althubeiti, M. Algethami, N. Rahman, M. Sohail, Q. Mao, Q. Zaman, A. Ullah, N. Ilyas and A. Afzal, *et al.*, Observation of quantum criticality in antiferromagnetic based $(Ce_{1-x}Y_x)_2Ir_3Ge_5$ Kondo-lattice system, *J. Magn. Magn. Mater.*, 2022, **556**, 169361.
8 N. Dimov, A. Nishimura, K. Chihara, A. Kitajou, I. D. Gocheva and S. Okada, Transition metal $NaMF_3$ compounds as model systems for studying the feasibility of ternary Li-MF and Na-MF single phases as cathodes for lithium–ion and sodium–ion batteries, *Electrochim. Acta*, 2013, **110**, 214–220.
9 J. Donaldson, S. G. Williams and S. Raymond, Characterization of a fluoroperovskite based fibre coupled optical dosimeter for radiotherapy, Annual Condensed matter and materials meeting, 2014.
10 K. Shimamura, T. Fujita, H. Sato, A. Bensalah, N. Sarukura and T. Fukuda, Growth and characterization of $KMgF_3$ single crystals by the Czochralski technique under CF_4 atmosphere, *Jpn. J. Appl. Phys.*, 2000, **39**, 6807.

11 A. Bensalah, K. Shimamura, K. Nakano, T. Fujita and T. Fukuda, Growth and characterization of $LiSrGaF_6$ single crystal, *J. Cryst. Growth*, 2001, **231**, 143–147.
12 M. Husain, M. S. Ahmad, N. Rahman, M. Sajjad, A. Rauf, A. Habib, H. Mahmood, M. Nisar, A. Hussain and M. Imran, *et al.*, First principle study of the structural, electronic, and Mechanical properties of cubic fluoroperovskites: ($ZnXF_3$, X = Y, Bi), *Fluoride*, 2020, **53**, 657–667.
13 M. S. Ahmad, A. Habib, A. Rauf, M. U. Haq, J. Saddique, M. Nisar, S. Shah, C. Maouche, S. Zulfiqar and M. U. Rehman, *et al.*, Theoretical investigation of the structural,electronic and mechanical properties of the magnesium-based fluoroperovskite compounds $XMgF_3$ (X = Ga, Al, In), *Theor. Invest.*, 2020, **1**, 542–553.
14 N. Rahman, M. Husain, J. Yang, M. Sajjad, G. Murtaza, M. U. Haq, A. Habib, R. A. Zulfiqar, A. Karim and M. Nisar, *et al.*, First principle study of structural, electronic, optical and mechanical properties of cubic fluoro-perovskites: ($CdXF_3$, X = Y, Bi), *Eur. Phys. J. Plus*, 2021, **136**, 1–11.
15 M. Harmel, H. Khachai, A. Haddou, R. Khenata, G. Murtaza, B. Abbar, S. Binomran and M. Khalfa, *Ab initio* study of the mechanical, thermal and optoelectronic properties of the cubic $CsBaF_3$, *Acta Phys. Pol.*, 2015, **128**, 34–42.
16 D. J. Daniel, U. Madhusoodanan, R. Nithya and P. Ramasamy, Irradiation effect on luminescence properties of fluoroperovskite single crystal ($LiBaF_3:Eu^{2+}$), *Radiat. Phys. Chem.*, 2014, **96**, 135–139.
17 M. Maqbool, I. Ahmad, H. Richardson and M. Kordesch, Direct ultraviolet excitation of an amorphous AlN: Praseodymium phosphor by codoped Gd^{3+} cathodoluminescence, *Appl. Phys. Lett.*, 2007, **91**, 193511.
18 G. Murtaza and I. Ahmad, Shift of indirect to direct bandgap and optical response of $LaAlO_3$ under pressure, *J. Appl. Phys.*, 2012, **111**, 123116.
19 G. Murtaza, I. Ahmad, B. Amin, A. Afaq, M. Maqbool, J. Maqssod, I. Khan and M. Zahid, Investigation of structural and optoelectronic properties of $BaThO_3$, *Opt. Mater.*, 2011, **33**, 553–557.
20 J. Saddique, M. Husain, N. Rahman, R. Khan, S. Zulfiqar, A. Iqbal, M. Sohail, S. Ali Khattak, S. Naz Khan and A. Ali Khan, *et al.*, Modeling structural, elastic, electronic and optical properties of ternary cubic barium based fluoroperovskites $MBaF_3$ (M = Ga and In) compounds based on DFT, *Mater. Sci. Semicond. Process.*, 2022, **139**, 106345.
21 G. K. Madsen, P. Blaha, K. Schwarz, E. Sjostedt and L. Nordstrom, Efficient linearization of the augmented plane-wave method, *Phys. Rev. B: Condens. Matter Mater. Phys.*, 2001, **64**, 195134.
22 J. P. Perdew, K. Burke and M. Ernzerhof, Generalized gradient approximation made simple, *Phys. Rev. Lett.*, 1996, **77**, 3865.
23 F. Tran and P. Blaha, Accurate band gaps of semiconductors and insulators with a semilocal exchange-correlation potential, *Phys. Rev. Lett.*, 2009, **102**, 226401.
24 F. Murnaghan, The compressibility of media under extreme pressures, *Proc. Natl. Acad. Sci. U. S. A.*, 1944, **30**, 244.
25 M. Jamal, M. Bilal, I. Ahmad and S. Jalali-Asadabadi, IRelast package, *J. Alloys Compd.*, 2018, **735**, 569–579.
26 J. Bechhoefer, Kramers–kronig, bode, and the meaning of zero, *Am. J. Phys.*, 2011, **79**, 1053–1059.
27 C. C. Kim, J. Garland and P. Raccah, Modeling the optical dielectric function of the alloy system Al_xGa_{1x} as, *Phys. Rev. B: Condens. Matter Mater. Phys.*, 1993, **47**, 1876.
28 P. Dufek, P. Blaha and K. Schwarz, Applications of Engel and Vosko's generalized gradient approximation in solids, *Phys. Rev. B: Condens. Matter Mater. Phys.*, 1994, **50**, 7279.
29 Z. Charifi, H. Baaziz, F. E. H. Hassan and N. Bouarissa, High pressure study of structural and electronic properties of calcium chalcogenides, *J. Phys.: Condens. Matter*, 2005, **17**, 4083.
30 M. A. Ali, N. Alam, S. Meena Ali, S. A. Dar, A. Khan, G. Murtaza and A. Laref, A theoretical study of the structural, thermoelectric, and spin-orbit coupling influenced optoelectronic properties of $CsTmCl_3$ halide perovskite, *Int. J. Quantum Chem.*, 2020, **120**, 26141.
31 A. Mohamed, A. El Houssine, F. Nejmaa and B. Ibrahim, *Ab initio* study of electronic, optical and thermoelectric properties of TiO2 phases using mBJ approximation, In Proceedings of the 2020 IEEE 6th International Conference on Optimization and Applications. ICOA 2020, pp. 1–5.
32 M. J. Mehl, Pressure dependence of the elastic moduli in aluminum-rich Al-Li compounds, *Phys. Rev. B: Condens. Matter Mater. Phys.*, 1993, **47**, 2493.
33 J. Wang, S. Yip, S. Phillpot and D. Wolf, Crystal instabilities at finite strain, *Phys. Rev. Lett.*, 1993, **71**, 4182.
34 R. Hill, The elastic behaviour of a crystalline aggregate, *Proc. Phys. Soc., London, Sect. A*, 1952, **65**, 349.
35 W. Voigt, *Lehrbuch der Kristallphysik (Textbook of crystal physics)*, BG Teubner, Leipzig and Berlin, 1928.
36 G. Ding, X. Chengwu, J. Bai, C. Zhenxiang, W. Xiaotian and W. Weikang, Recipe for single-pair-Weyl-points phonons carrying the same chiral charges, *Phys. Rev. B*, 2023, **108**, L020302.
37 G. Ding, X. Chengwu, G. Jialin, J. Wang, J. Bai, W. Wang, D. Li, X.-P. Li and X. Wang, Exotic topological phonon modes in semiconductors: Symmetry analysis and first-principles calculations for representative examples, *Phys. Rev. B*, 2023, **108**, 075201.
38 A. A. A. Russ, The origin of rheology, *Mater. Phys.* 1929, 49.
39 D. Pettifor, Theoretical predictions of structure and related properties of intermetallics, *Mater. Sci. Technol.*, 1992, **8**, 345–349.
40 S. X. C. I. I. Pugh, Relations between the elastic moduli and the plastic properties of polycrystalline pure metals, *London, Edinburgh Dublin Philos. Mag. J. Sci.*, 1954, **45**, 823–843.
41 I. Frantsevich, Elastic constants and elastic moduli of metals and insulators hand book, In Reference Book, 1982.
42 D. R. Penn, Electron mean-free-path calculations using a model dielectric function, *Phys. Rev. B: Condens. Matter Mater. Phys.*, 1987, **35**, 482.

43 M. Naseri, J. Jalilian and A. H. Reshak, Electronic and optical properties of pentagonal-B2C monolayer: a first-principlescalculation, *Int. J. Mod. Phys. B*, 2017, **31**, 1750044.
44 J. Wang, H. Yuan, Y. Liu, X. Wang and G. Zhang, Multiple dimensions of spin-gapless semiconducting states in tetragonal Sr_2CuF_6, *Phys. Rev. B*, 2022, **106**, L060407.
45 J. Wang, H. Yuan, W. Wang, G. Ding, X.-P. Li and X. Wang, Fully spin-polarized hourglass charge-three Weyl points and sextuple-helicoid surface arcs in P6322-type $BaNiIO_6$, *Phys. Rev. B*, 2023, **108**, 054424.